Synthesis and Characterization of Poly(vinylpyrrolidone)-Modified Zinc Oxide Nanoparticles

Lin Guo and Shihe Yang*

Department of Chemistry, The Hong Kong University of Science and Technology, Clear Water Bay, Kowloon, Hong Kong

Chunlei Yang, Ping Yu, Jiannong Wang, Weikun Ge, and George K. L. Wong

Department of Physics, The Hong Kong University of Science and Technology, Clear Water Bay, Kowloon, Hong Kong

Received December 16, 1999. Revised Manuscript Received May 22, 2000

We have synthesized highly monodisperse wurtzite ZnO nanoparticles using poly(vinylpyrrolidone) (PVP) as the capping molecules. The effect of surface modification on the size, structure, morphology, and optical properties of ZnO nanoparticles was investigated. It was found that many properties of the ZnO nanoparticles could be optimized by simply varying the molar ratio Zn(II)/PVP. The ZnO nanoparticles prepared under the optimum conditions are particularly stable, monodisperse, as well as small in size. The EXAFS result showed a structural contraction in the ZnO nanoparticles relative to the bulk. These nanoparticles exhibit distinct excitonic absorption features, markedly enhanced near-band-edge UV photoluminescence, and significantly reduced defect-induced green emission. The third-order nonlinear optical response of these PVP-capped ZnO nanoparticles in a dilute solution was found to be larger than that of the bulk ZnO by at least 2 orders of magnitude.

Introduction

As a semiconductor material, zinc oxide spans a wide range of applications from solar cells[1] and chemical sensors,[2] to electrical, acoustic, and luminescent devices.[3−5] Recently, ZnO has attracted increasing interest due to its relatively high efficiency as a low-voltage phosphor. It is considered to be a promising phosphor for low-voltage luminescence in flat panel displays.[6,7] To keep abreast of the industry for flat panel displays and other optical devices, the luminescence efficiency of ZnO must be substantially improved.[8]

Various methods have been adopted for the preparation of zinc oxide particles, which include the sol−gel method,[9] the evaporation of solutions and suspensions, evaporative decomposition of solutions (EDS), conventional ceramic fabrication, and wet chemical synthesis. In recent years, several new techniques for preparing nanosized ZnO particles and films have been developed. Among them is a novel method of synthesizing ZnO colloids of wurtzite nanocrystals as reported by Spanhel et al.,[10] Bahnemann and co-workers,[11] and Henglein and co-workers.[12,13] In addition, studies on the structure−property relationships of ZnO nanocrystals have also started to appear.[14,15]

There have been virtually no reports on the synthesis of surfactant- or polymer-stabilized ZnO nanoparticles. Although dodecyl benzene sulfonate (DBS) and poly(vinylpyrrolidone) (PVP) were used to stabilize ZnO nanoparticles,[16,17] the size distribution and the surface microstructures were unclear. In addition, the optical properties of these DBS-stabilized ZnO nanoparticles were not investigated in detail. It has been well-established that stabilization and surface passivation of nanoparticles are vitally important for the development of electrical and optical materials based on these nanoparticles. To this end, we have recently synthesized nearly monodisperse ZnO wurtzite nanocrystals stabilized by

* Corresponding author. E-mail: chsyang@ust.hk.

(1) *Thin Film Solar Cells*; Chopra, K. L.; Das, S. R., Eds.; Plenum: New York, 1983.
(2) Muller, J.; Fresenius, S. W. *J. Anal. Chem.* **1994**, *349*, 380.
(3) Hingorani, S.; Pillai, V.; Kumar, P.; Multani, M. S.; Shah, D. O. *Mater. Res. Bull.* **1993**, *28*, 1303.
(4) Kong, L. B.; Li, F.; Zhang, L. Y.; Yao, X. *J. Materials Science Letters*, **1998**, *17*, 769.
(5) Shih, W. C.; Wu, M. S. *J. Cryst. Growth*, **1994**, *137*, 319.
(6) Troy, C. T. *Photonics Spectra* **1997**, *31*, 34.
(7) Vanheusden, K.; Seager, C. H.; Warren, W. L.; Tallant, D. R.; Caruso, J.; Hampden-Smith, M. J.; Kodas, T. T. *J. Lumines* **1997**, *75*, 11.
(8) Mo, C. M.; Li, Y. H.; Lin, Y. S.; Zhang, Y.; Zhang, L. P. *J. Appl. Phys.* **1998**, *83*, 4389.
(9) Lauf, R. J.; Bond, W. D. *Ceram. Bull.* **1984**, *63*, 278.
(10) Spanhel, L.; Anderson, M. A. *J. Am. Chem. Soc.* **1991**, *113*, 2826.
(11) Bahnemann, D. W.; Karmann, C.; Hoffmann, M. R. *J. Phys. Chem.* **1987**, *91*, 3789.
(12) Koch, U.; Fojtik, A.; Weller, H.; Henglein, A. *Chem. Phys. Lett.* **1985**, *122*, 507.
(13) Haase, M.; Weller, H.; Henglein, A. *J. Phys. Chem.* **1988**, *92*, 482.
(14) Sakohara, S.; Ishida, M.; Anderson, M. A. *J. Phys. Chem.* B **1998**, *102*, 10169.
(15) E. A. Meulenkamp, E. A. *J. Phys. Chem.* B **1998**, *102*, 7764.
(16) Wang, R.; Wu, X. C.; Zou, B. S.; Xu, J. R.; Wang, L.; Wu, P. F.; Liu, S. M.; Wang, J. G. *Chinese Phys. Lett.* **1998**, *15*, 27.
(17) Mahamuni, S.; Bendre, B. S.; Leppert, V. J.; Smith, C. A.; Cooke, D.; Risbud, S. H.; Lee, W. H. W. *Nanostruct. Mater.* **1996**, *7*, 659.

10.1021/cm9907817 CCC: $19.00
Published on Web 07/11/2000

Scheme 1

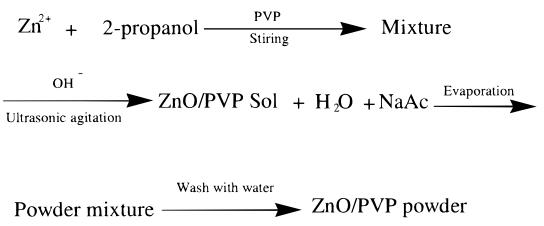

PVP with a particle size of a few nanometers, and characterized their linear and nonlinear optical properties under different surface capping conditions with PVP. A preliminary report on the PVP-capped ZnO nanoparticles has been given elsewhere.[18] In the present paper, we provide a full description of this work and its extension.

Experimental Section

ZnO Nanoparticle Synthesis. The synthetic procedures for the surface-modified ZnO nanoparticles are briefly summarized in Scheme 1. The polymer PVP (ACROS, MW 10 000) was introduced as a capping molecule for the ZnO nanoparticles. It serves to stabilize the ZnO nanoparticles and passivate the surface to reduce the oxygen vacancy sites.

Zinc acetate ($(CH_3COO)_2Zn{\cdot}2H_2O$, from Aldrich, 0.5 mmol) was dissolved in 80 mL of 2-propanol under vigorous stirring at 50 °C. The solution was diluted to a total volume of 920 mL, followed by chilling to 0 °C. The resulting solution was divided into four aliquots, each of which was contained in a separate flask. PVP was added into the above flasks under vigorous stirring to prepare four solutions with the molar ratios Zn(II)/PVP being 5:0, 5:1, 5:3, and 5:5, respectively at room temperature. The mixtures were then hydrolyzed in an ultrasonic bath at room temperature by the following procedures: 50 mL of a 2×10^{-2} mol/L NaOH solution (GR grade) in 2-propanol (HPLC grade) was added dropwise to each of the above four diluted and cooled precursor solutions using a separation funnel, and the reaction was maintained for ~2 h. Finally, four ZnO nanoparticle solutions were obtained, labeled as sample 1, 2, 3, and 4, respectively. To examine the effect of the molar ratio Zn(II)/PVP on the nanoparticle properties in a broader range, we prepared another sample following exactly the same procedure as described above but with the molar ratio Zn(II)/PVP = 5:8 (labeled as sample 5). The samples were stored at room temperature for measurements of optical absorption, steady-state photoluminescence, and nonlinear optical properties.

For X-ray diffraction (XRD) and EXAFS experiments, powder samples were used. The powder samples were prepared by removing the solvent using a rotary evaporator, washing the resulting powder mixture three times with high-purity water ($\rho > 18$ MΩ cm^{-1}), and drying it in a vacuum at room temperature.

Structural Characterization. The size and shape of the ZnO nanoparticles were determined using a JEOL 2010 high-resolution transmission electron microscope (HRTEM). The microscope, operated at 200 keV, has a spatial resolution of 0.17 nm. Samples were prepared by placing a drop of the colloidal suspension on holey carbon-coated copper grids, the excess solvent was evaporated, and the sample was dried in a vacuum.

Crystal structure identification was carried out by X-ray diffraction using a PHILIP 8338 model diffractometer with Cu Kα incident radiation. The samples for X-ray diffraction measurements were prepared by rotary evaporation of the ZnO nanoparticle suspension to a fine powder. The ZnO nanoparticle powder was collected and then dried in a vacuum oven at 100 °C for ~2 h.

XAFS spectra were collected in the XAFS station (beam line 4W1B) of the Beijing Synchrotron Radiation Laboratory. The ZnO nanoparticles were homogeneously smeared on adhesive tape. More than eight layers were folded to reach the optimum absorption thickness ($\Delta\mu d \approx 1.0$, where d is the physical thickness of the sample and μ is the linear absorption coefficient). X-ray absorption spectra (near the Zn−K edge) of bulk ZnO and nanoscale ZnO particles modified by PVP were collected, respectively, at ambient temperature in the transmission mode. The storage ring was run at 2.2 GeV with an electron current of ~50 mA. High harmonics of the X-ray were eliminated by detuning the double crystal Si(111) monochromator with a ~40% decrease of the fundamental wave intensity. The incident and transmitted X-ray intensities were detected, respectively, by ion chambers installed in front of and behind the sample. The X-ray photon energies were calibrated by taking the inflection point on the Cu−K absorption edge to be 8980.3 eV, which is from the literature.[19] The energy resolution at the Zn−K absorption edge was ~2 eV. The absorption spectra were collected from 200 eV below the absorption threshold to over 1000 eV above the absorption threshold. The collection time for each data point was 1 s.

Optical Measurements. Optical absorption spectra were recorded on a Philips 3000 spectrophotometer. In these experiments, appropriate blank solutions of pure 2-propanol and PVP/2-propanol mixtures were used as references for the samples 1, 2, 3, 4, and 5, respectively. Photoluminescence (PL) spectra were recorded using a He−Cd laser as the excitation light source at room temperature. A Spex500 spectrometer, a photomultiplier tube (PMT), and a photon counter were used as the detection system.

The nonresonant third-order nonlinear susceptibility [$\chi^{(3)}$] was measured by using a degenerate four-wave-mixing technique (DFWM) in a forward geometry. The light source was the second harmonic of a Q-switched, mode-locked Nd:YAG laser (532 nm). The laser was operated at a repetition rate of 500 Hz and the pulse width of the individual pulses was about 70 ps. The probe beam was incident at an angle of 2° with respect to the forward pump beam. The conjugate signals were detected using a sensitive Si photodiode and a lock-in amplifier.

Results and Discussion

Morphology and Structure. The PVP-capped ZnO nanoparticles are in general more stable than the noncapped nanoparticles. For example, the PVP-capped ZnO nanoparticle solutions did not show any observable change after more than half a year, whereas the noncapped ZnO nanoparticles precipitated from the solution after storage for only 2 months at room temperature. In terms of appearance, the samples 1−4 are colorless, but sample 5 is greenish yellow.

Typical HRTEM images of the ZnO nanoparticles are shown in Figure 1 for samples 1 and 3. Direct comparison of the two TEM images shows that the noncapped ZnO nanoparticles are prone to aggregation, whereas the PVP-capped nanoparticles are well-separated with no sign of aggregation. Notably, the ZnO nanoparticles that were modified by PVP have a very narrow size distribution compared with those without PVP modification. In particular, the ZnO nanoparticles in sample 3 with the ratio of Zn(II)/PVP = 5:3 are nearly monodisperse. The mean particle sizes are estimated to be 4.0 ± 0.5, 3.6 ± 0.5, 2.6 ± 0.3, and 2.8 ± 0.4 nm, respectively, for the PVP-modified ZnO nanoparticle samples 1−4. It follows that the ZnO nanoparticles in sample 3 with the ratio of Zn(II)/PVP = 5:3 have the

(18) Guo, L.; Yang, S. H.; Yang, C. L.; Yu, P.; Wang, J. N.; Ge, W. K.; Wong, G. K. L. *Appl. Phys. Lett.* **2000**, *76*, 2901.

(19) Wu, Z. H.; Guo, L. *J. Synchrotron Radiat.* **1999**, *6*, 749.

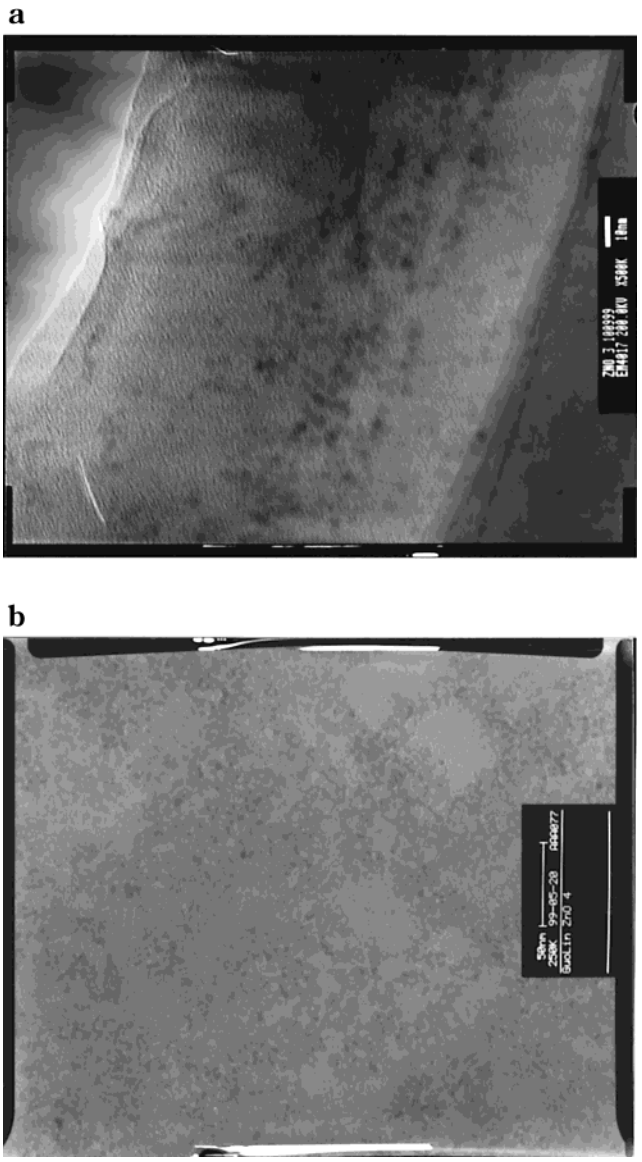

Figure 1. TEM pictures of ZnO nanoparticles in sample 1 (a) and sample 3 (b).

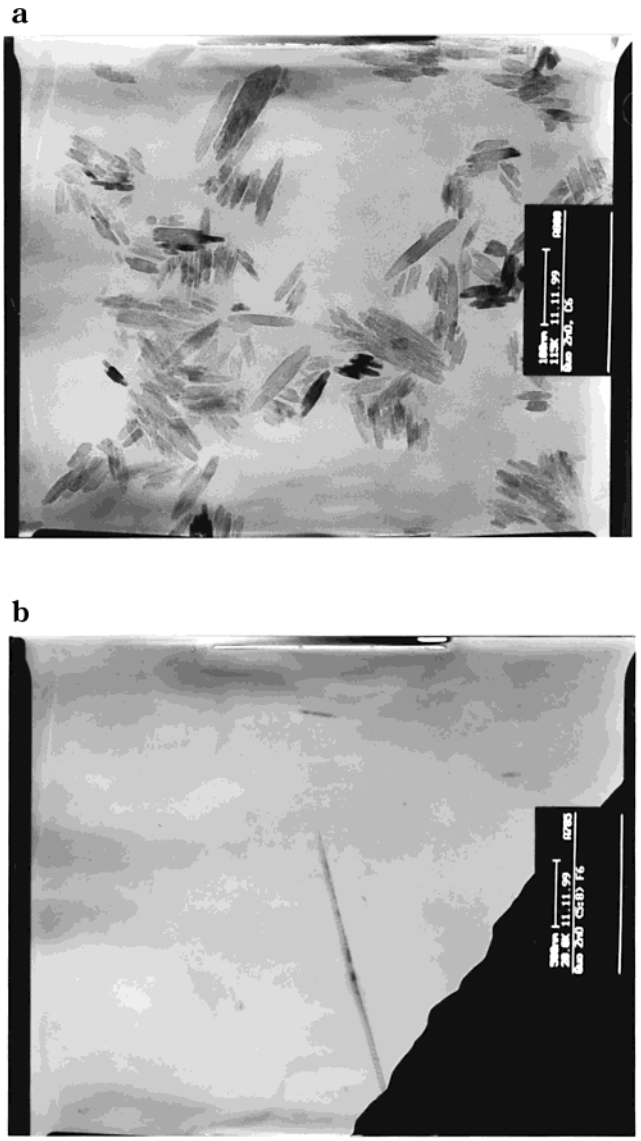

Figure 2. TEM pictures of ZnO nanoparticles in sample 5: (a) overview and (b) a single nanofiber.

smallest particle size (~2.6 nm) of all four samples. Furthermore, the ZnO nanoparticles that were not modified by PVP (sample 1) appear to be ellipsoid in shape, presumably due to aggregation, while those from the PVP-modified samples 2−4 are spherical in shape.

When the molar ratio of Zn(II)/PVP decreases further to 5:8, the morphology of the ZnO nanoparticles changes dramatically. Figure 2 displays the TEM images of the ZnO nanoparticles (sample 5). Instead of the spherical or pseudospherical particles, extended one-dimensional rods are observed. These rods are closely packed together in most cases. The single rods are typically 15 nm thick and 55 nm long with an aspect ratio of ~4 (Figure 2a). The longest ZnO rods are ~2 μm in length and ~40 nm in thickness (Figure 2b). We have not yet succeeded in taking a high-resolution TEM picture and powder X-ray diffraction pattern of these interesting structures. The mechanism for the formation of the rods remains to be investigated, but it is clear that the PVP molecules play a significant role in the process.

The changes in morphology and size of the ZnO nanoparticles as a function of the molar ratio of Zn(II) show that the role of PVP is evident. When no capping molecules are introduced, particle interaction and aggregation are inevitable, accounting for the instability of sample 1. The presence of capping molecules appears to affect the kinetics of nucleation and accretion in such a way that the growth of large particles slows down while the growth of small particles remains about the same. This would in effect narrow the nanoparticle size distribution, as observed in samples 3 and 4. However, as the PVP concentration increases further, the interaction between PVP molecules becomes important. This may encourage structured phases, which favor the rod formation, as seen in sample 5.

Figure 3 shows the powder X-ray diffraction pattern of ZnO nanoparticles (sample 3). The diffraction pattern and interplane spacings can be well-matched to the standard diffraction pattern of wurtzite ZnO, demonstrating the formation of wurtzite ZnO nanocrystals. The particle size was calculated using the Debye−Scherer formula, $t = 0.89\lambda/(\beta \cos \theta_B)$, where λ is the X-ray wavelength (1.5406 Å), θ_B is the Bragg diffraction angle, and β is the peak width at half-maximum. The XRD peaks at 47.42° and 56.41° in Figure 2 give the

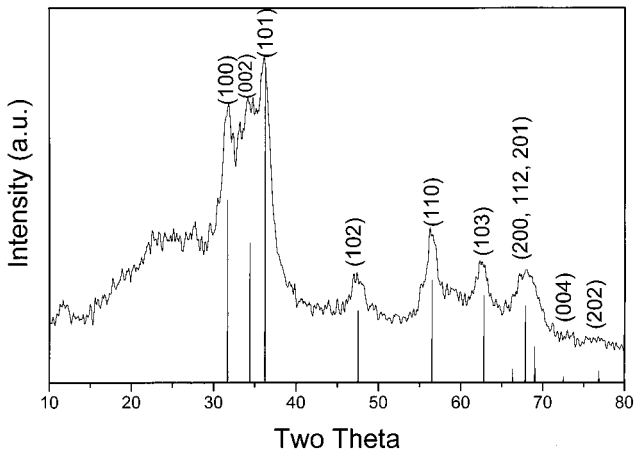

Figure 3. X-ray diffraction pattern of the ZnO nanoparticles (sample 3). The vertical lines indicate the diffraction peaks of bulk Wurtzite ZnO.

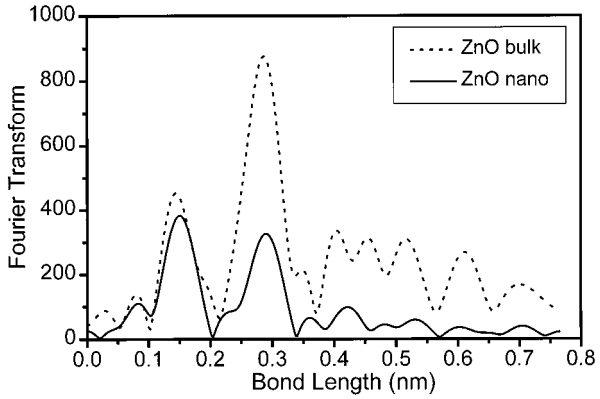

Figure 4. Fourier transformed spectra (Zn K absorption) of the bulk ZnO (broken line) and PVP-coated ZnO nanoparticles (solid line).

ZnO particle diameters of 2.66 and 2.88 nm, respectively. These estimates are quite consistent with the diameter value obtained above from the TEM analysis (~2.6 nm).

In the X-ray absorption experiments of the ZnO nanoparticles (sample 3), the preedge absorption background was fitted and subtracted by using the Victoreen formula.[20] The half-height of the edge-jump was chosen as the energy threshold. The spline function was used to derive the EXAFS signal and remove the postedge absorption background.[19] EXAFS functions were normalized by using the absorption edge-jump and were Fourier transformed to the R space with the k^3-weight in the range of 2.52−9.27 Å^{-1}. Fourier filters were performed in the range of 0.96−2.04 Å. Five fitting parameters are allowable. Hanning windows were used in the Fourier transform and the filtering process.[21] The Fourier transformed spectra of the ZnO bulk (broken line) and nanoparticle (solid line) samples are both shown in Figure 4.

The experimental near-neighbor coordination EXAFS function of the ZnO nanoparticle sample is plotted in Figure 5 (dotted line). A single coordination shell was used to fit the Zn K-absorption EXAFS signal of the ZnO nanoparticles. The following EXAFS formula was used to fit the experimental spectrum:[21]

$$\chi_i(k) = \frac{{s_0}^2 N_j}{kR_j^2} F_j(\pi,k) \exp(-2k^2\Delta{\sigma_j}^2) \exp(-2R_j/\lambda_j) \sin(2kR_j + \phi_j) \quad (1)$$

Here N_j neighbors stand at a distance R_j away from the absorber. $F_j(\pi,k)$ is the backscattering factor, and ${s_0}^2$ is the reduction factor. λ_j is the mean free path of the photoelectron and ϕ_j is the phase shift. $\Delta{\sigma_j}^2 = {\sigma_{uj}}^2 - {\sigma_{sj}}^2$, where the subscripts u and s, respectively, stand for the unknown and reference samples.

The backscattering amplitude $[A_s(\pi,k) = {s_0}^2 F(\pi,k) \exp(-2k^2{\sigma_s}^2) \exp(-2R_s/\lambda_s)]$ and the phase shift (ϕ_s) of the Zn−O bonds were calculated by using an FEFF code according to the zinc blende-type crystal structure of bulk ZnO.[22] Due to the transferability of the backscattering amplitude and the phase shift, they were substituted for those of the unknown ZnO nanoparticle samples in eq 1. The fitting curve to the experimental EXAFS function of the ZnO nanoparticle sample is also shown in Figure 5 (solid line). Table 1 tabulates the fitting parameters. From Table 1, we can see that there are about 4.0 and 3.5 O atoms around Zn on average with the Zn−O distance of 2.007 and 1.97 Å, for bulk ZnO and ZnO nanoparticles, respectively. The decrease in the average coordination number for the ZnO nanoparticles compared with that of the bulk ZnO is evident and can be attributed to the decrease in the particle size and the increase in the surface-to-volume ratio. Although part of the Zn atoms on the ZnO nanoparticle

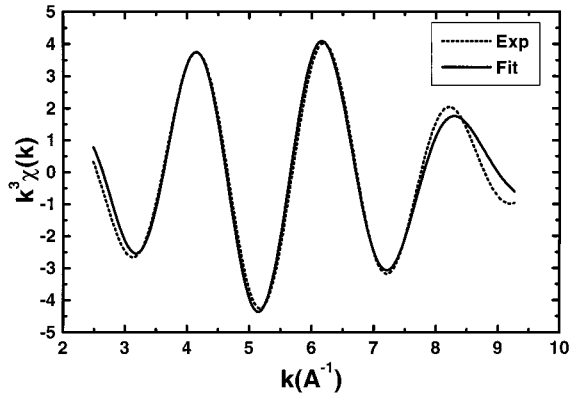

Figure 5. Experimental (dotted line) and fitted (solid line) EXAFS curves with k^3-weighting of the Zn−O coodination numbers in the ZnO nanoparticles capped by PVP.

Table 1. Structural Parameters of Zn−O Bonds in the ZnO Nanoparticles[a]

samples	N	R (Å)	σ^2 (Å^2)	ΔE_0
ZnO bulk	4	2.00	0.0050	0
ZnO nano	3.5	1.97	0.0062	−4.51

[a] N is the oxygen coordination number around the zinc atom; R is the bond length of Zn−O; σ^2 is the Debye−Waller factor; ΔE_0 is the shift of energy threshold. A standard sample was used as the reference for which the EXAFS curve with k^3-weighting was calculated by using the FEFF5.04 code.

(20) Wu, Z. H.; Guo, L.; Li, Q. S.; Zhu, H. S. *J. Phys., Cond. Matter* **1999**, *11*, 4961.

(21) Sayers, D. E.; Bunker, B. A. In *X-ray Absorption: Principle, Applications and Techniques of EXAFS, SEXAFS and XANES*; edited by Koningsberger, D. C., R. Prins, R., Eds.; Wiley: New York, 1988; Chapter 6, p 226.

(22) Abraham, S. C.; Bernstein, J. L. *Acta Cryst.* B **1969**, *25*, 1233.

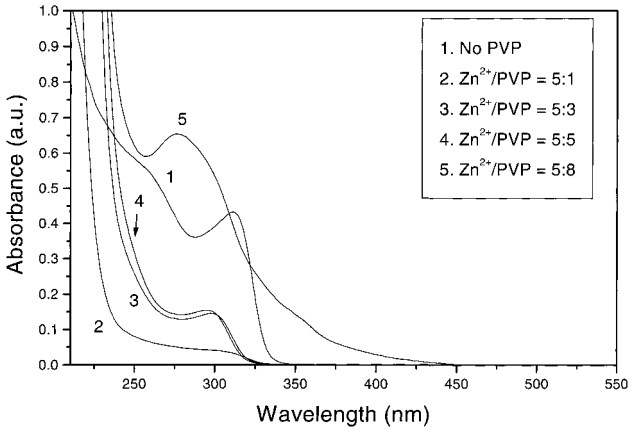

Figure 6. Optical absorption spectra of the ZnO nanoparticles (samples 1−5).

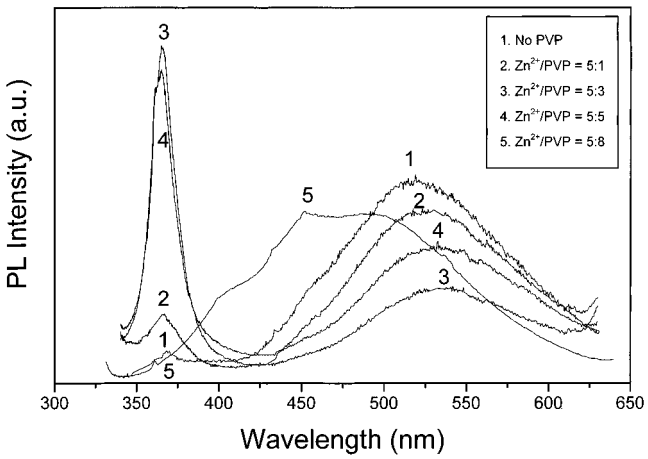

Figure 7. Photoluminescence spectra of the ZnO nanoparticles (samples 1−5).

surfaces are probably capped by the carboxylate groups of PVP, their coordination is still likely to be unsaturated. This explains the decrease in the average coordination number for the ZnO nanoparticles from that for the bulk ZnO. The Zn−O bond length in the nanoparticles is slightly shorter than that in the bulk ZnO, indicating a structural contraction for the nanoparticles. This demonstrates that the interaction between oxygen and zinc is stronger in these nanosized ZnO samples than in the bulk ZnO. A similar result was reported by Kessler and co-workers for ZnO nanoclusters confined inside the cages of Sodalite.[23]

Optical Properties. Presented in Figure 6 are room temperature optical absorption spectra of ZnO nanocrystals prepared using different molar ratios of Zn(II)/PVP. Common to all the spectra are the strong exciton absorption features owing to the relatively large exciton binding energy (∼60 meV in bulk ZnO)[24] and the significant blue shifts of these features (∼300 nm) relative to the bulk exciton absorption (373 nm).[13] This confinement effect is consistent with the small size of the ZnO nanoparticles we prepared. However, depending on the molar ratio of Zn(II)/PVP used to prepare the ZnO nanoparticles, significant differences can be recognized among the spectra. First, with the decrease of the Zn(II)/PVP ratio, the excitonic absorption peak shifts consistently to shorter wavelengths. Specifically, the excitonic feature appears at 312 nm for the sample with no PVP modification and at 306, 301, and 297 nm for the PVP-modified ZnO nanoparticle samples 2, 3, and 4, respectively. This is likely to be due to the nanoparticle size reduction following this order. For sample 5, however, the onset absorption shifts significantly to the red (>500 nm), and the absorption increases very slowly with decreasing wavelength. A blank experiment was conducted to determine whether the green-yellow color of sample 5 originates from reactions of PVP in the presence of base (e.g., pyrrolidone ring opening reaction). With the same concentration of PVP and NaOH as in the sample 5 but without Zn, the solution is still colorless. Therefore, the green-yellow color of sample 5 appears to be due to the presence of Zn^{2+}. We believe that the color of sample 5 is associated with ZnO nanorods because only this sample shows abundant formation of extended ZnO nanorods (Figure 2b). Actually, the sloppy absorption onset of sample 5 (Figure 6) is characteristic of one-dimensional semiconductor materials. Second, there is a bump immediately to the blue side of the excitonic absorption peak in sample 1 (∼260 nm) and sample 5 (∼280 nm), but not in the other samples. This indicates a broader size distribution of ZnO nanoparticles in these two samples as compared with other samples.

From the absorption onsets in Figure 6, we can also calculate the ZnO nanoparticle diameter of each sample based on the effective mass approximation.[25] The estimated diameters of the ZnO nanoparticles using this approach are 3.83, 3.59, 3.31, and 3.28 nm for samples 1−4, respectively. These results, again, are remarkably close to those obtained from both the TEM observation and the XRD analysis given the crudeness of the model.

The photoluminescence spectra of the five samples, which were recorded with the excitation wavelength set at 325 nm, are shown in Figure 7. All the above samples except for sample 5 evince two emission bands: one is at ∼365 nm and the other is at ∼530 nm. The UV emission peak was regarded as being from the band gap luminescence of the ZnO nanoparticles.[10,13,26] Although its exact nature is still controversial, the green peak was generally attributed to the deep trap mediated luminescence.[10,13,26,27] The relative intensities of these two emission bands vary dramatically with the molar ratio of Zn(II)/PVP, as do the exact locations of these two bands, albeit to a much smaller extent. Sample 5 exhibits only a broad PL feature around 480 nm.

In general, the UV emission peak increases when the ZnO nanoparticles are capped with PVP, with the exception of sample 5. In the noncapped sample (1), the UV peak is quite weak. In samples 3 and 4, however, the UV peak is strong and sharp (fwhm = ∼19 nm). Although this peak was previously observed by other researchers at a similar wavelength,[20,28] its intensity

(23) Khouchaf, L.; Tuilier, M. H.; Durr, J.; Wark, M.; Kessler, H. *J. Phys.* IV **1996**, *6*, C4−939.
(24) Tang, Z. K.; Wong, G. K. L.; Yu, P.; Kawasaki, M.; Ohtomo, A.; Koinuma, H.; Segawa, Y. *Appl. Phys. Lett.* **1998**, *72*, 3270.
(25) Wong, M. E.; Bonevich, J. E.; Searson, P. C. *J. Phys. Chem.* B **1998**, *102*, 7770.
(26) Monticone, S.; Tufeu, R.; Kanaev, A. V. *J. Phys. Chem. B* **1998**, *102*, 2854.
(27) Studenikin, S. A.; Golego, N.; Cociera, M. *J. Appl. Phys.* **1998**, *184*, 2287.

was weak compared with that of the broad visible bump. The strong UV luminescence we observed demonstrates the good quality of the ZnO nanoparticles in samples 3 and 4. The sharpness of the UV peak also shows that the ZnO nanoparticle sizes in these samples are nearly monodisperse, as revealed earlier by TEM. However, the UV emission of sample 2 is much weaker than that of samples 3 and 4. Still weaker UV emission occurred in sample 1; it was ~2.5 and ~11 times weaker than that of samples 2 and 3, respectively. In addition, the UV peak positions of samples 1 (370 nm) and 2 (368 nm) are somewhat shifted toward red when compared with those of sample 3 (364 nm) and 4 (365 nm), probably due to their slightly larger sizes. Sample 5 does not show an observable UV emission peak presumably due to the morphological change from spherical particles to nanorods.

It is worth noting that the UV peak is shifted toward red by as much as ~70 nm (~0.78 eV) from the absorption onset (Figure 7). The large red shift (~0.78 eV) seems not to be explicable by simple electron−phonon coupling because it requires too large a Huang−Rhys parameter *S*. Surface shallow traps or dark excitons arising from the lift of the degeneracy of the exciton fine structure levels may explain the UV emission peak as proposed by recent theory and experiments.[28,29]

The broad photolumunescence band of the ZnO nanoparticles at ~530 nm that we observed (see Figure 4) has actually been reported by many other research groups.[8,11,12,20,30,31] This broad bump (~530 nm) appears in the photoluminescence spectra of all five ZnO nanoparticle samples that we prepared. However, the intensity of this peak relative to that of the UV luminescence changes drastically with the molar ratio of Zn(II)/PVP. Initially, the green peak intensity decreases with the decreasing molar ratio of Zn(II)/PVP in samples 1−3, but further decreases in Zn(II)/PVP result in an increase of the green photolumunescence intensity (samples 4 and 5). Another feature about the green luminescence peak is that the peak position shifts to short wavelengths from ~538 to ~510 nm in samples 3, 4, 2, and 1 following this order. In sample 5, the broad visible PL bump consisting of four peaks at ~400, ~430, ~450, and ~495 nm is the only feature we observed, which is significantly shifted toward blue relative to that of the other four samples. In general, in all five ZnO nanoparticle samples, a more intense UV luminescence peak correlates very well with a lower intensity and a longer peak wavelength of the green emission bump. Consequently, sample 3 possesses the highest intensity ratio of the UV luminescence peak to the green luminescence peak.

As mentioned above, a lot of effort has been spent to understand the mechanism for the green emission band. Heglein et al. attributed it to surface anion vacancies.[12] Behneman and co-workers proposed a mechanism that involves tunneling of surface-bound electrons to preexisting trapped holes.[11] Recently, Monticone et al.[32] and Mo et al.[8] accounted for the green emission band in terms of defect levels associated with oxygen vacancies or zinc interstices. Our experimental result shows clearly the role of the PVP capping molecules in reducing the defects or traps. These defects or traps are most probably on the nanoparticle surfaces, where the PVP molecules have the most direct and efficient passivation effect. Furthermore, we believe that the green emission originates from the oxygen anion vacancy on the surface of the ZnO nanoparticles as proposed by other researchers.[26,27,30] It is likely that the surface passivation may at least partially eliminate the surface trap states, and the PVP-capped-ZnO nanoparticles should therefore have weaker green emissions and correspondingly stronger UV emissions. Another interesting phenomenon is that the higher the green peak is, the shorter the wavelength of the peak is. As we know, surface trap states are inhomogeneous. It is difficult to imagine that all the surface traps have exactly the same removal probability by PVP. A likely scenario is that the shallower the trap states, the easier they will be removed by PVP. This line of reasoning can naturally explain the red shift of the green emission band induced by PVP capping.

The PL data presented above suggest that there is an optimum PVP concentration for the minimum green emission and maximum UV emission. We believe further optimization efforts can completely eliminate the green emission. The reason for the revival of the green emission at higher PVP concentrations is perhaps due to the interaction between the PVP molecules themselves and the consequently poor uniformity of the ZnO nanocrystal size and surface structure.

Nonlinear optical properties of the ZnO nanoparticles (sample 3) were investigated using DFWM at room temperature with a picosecond pulsed laser at 532 nm. Carbon disulfide was used as the reference for the quantitative measurements of the nonresonant, third-order susceptibilities $\chi^{(3)}$ of the ZnO nanoparticles. The $\chi^{(3)}$ value of the chemically derivatized ZnO nanoparticles by PVP was calculated by comparing the conjugate signal of the ZnO nanoparticles with that of the reference CS_2 ($\chi^{(3)} = 2.3 \times 10^{-13}$ esu) [33] using the equation[34,35]

$$\chi_s^{(3)} = \chi_{ref}^{(3)} \frac{n_s^2}{n_{ref}^2} \sqrt{\frac{I_{4s}}{I_{4ref}}} \sqrt{\frac{P_{ref}^3}{P_s^3}} \frac{\alpha e^{\alpha L_{effs}/2}}{(1 - e^{-\alpha L_{effs}})} L_{effref} \quad (2)$$

where L_{effs} and L_{effref} are, respectively, the path lengths of the ZnO nanoparticle sample solution and of the reference solvent, n is the refractive index, α is the absorption coefficient of the sample, I_4 is the DFWM intensity, and P is the average laser power. In eq 2, the subscript s represents the ZnO nanoparticle samples and ref represents the reference CS_2.

The $\chi^{(3)}_{composite}$ value of the ZnO nanoparticles capped by PVP in 2-propanol at a ZnO concentration of 5×10^{-4} M was estimated from the above equation. The true $\chi^{(3)}_{ZnO}$ value of the ZnO nanoparticles at this

(28) Smith, C. A.; Lee, H. W. H.; Leppert, V. J.; Risbud, S. H. *Appl. Phys. Lett.* **1999**, *75*, 1688.
(29) Kuno, M.; Lee, J. K.; Dabbousi, B. O.; Mikulec, F. V.; Bawendi, M. G. *J. Chem. Phys.* **1997**, *106*, 9869.
(30) Sakohara, S.; Ishida, M.; Anderson, M. A. *J. Phys. Chem.* B **1998**, *102*, 10169.
(31) Wong, M. E.; Searson, P. C. *Appl. Phys. Lett.* **1999**, *74*, 2939.
(32) Smith, C. A.; Lee, H. W. H.; Leppert, V. J.; Risbud, S. H. *Appl. Phys. Lett.* **1999**, *75*, 1688.
(33) Minoshima, K. *Opt. Lett.* **1991**, *16*, 1683.
(34) Sutherland, R. L. *Handbook of Nonlinear Optics*; Marcel Dekker: New York, 1996; p 298 and 389.
(35) Puech, K. *Opt. Lett.* **1995**, *20*, 1613.

concentration was obtained by subtracting the $\chi^{(3)}_{blank}$ value of PVP in 2-propanol (a very small contribution to $\chi^{(3)}_{composite}$) from the $\chi^{(3)}_{composite}$ value. In this way, $\chi^{(3)}_{ZnO}$ can be calculated, and the final result is 6.3×10^{-11} esu. This value is more than two orders of magnitude larger than that of the bulk ZnO sample,[36] a remarkable enhancement of the third-order nonlinear optical nonlinearity, which is likely due to the exciton confinement and optical Stark effect.[16,37]

Summary

Wurtzite ZnO nanocrystals were synthesized as a remarkably stable organosol using the polymer PVP for surface passivation. The effect of the starting molar ratio of Zn(II)/PVP on the ZnO nanoparticles was investigated. It has been demonstrated that the ratio of Zn(II)/PVP = 5:3 gave rise to ZnO nanopaparticles with the narrowest size distribution. Surprisingly, increasing the molar ratio of Zn(II)/PVP eventually leads to the formation of ZnO nanorods. The EXAFS result showed that with a decrease in the ZnO nanoparticle size, the coordination number decreases. Because the interaction between oxygen and zinc is stronger in these nanosized materials than in bulk ZnO, the Zn−O bond length is slightly shorter than that in the bulk ZnO, indicating a structural contraction in the ZnO nanoparticles.

Quantum size effects are evident from the optical absorption spectra, which showed blue shifts in the excitonic feature from the value of bulk ZnO by ~70 nm. For the ZnO nanoparticle sample prepared with the molar ratio of Zn(II)/PVP = 5:3, the most intense near-band-edge luminescence was observed with only a weak green luminescence, whereas the green luminescence was significantly enhanced at the expense of the near-band-edge luminescence in the ZnO nanoparticle sample with no PVP modification. This result leads us to believe that the green emission is due to the surface traps, e.g., oxygen vacancy. In addition, the UV emission band may be ascribed to surface shallow traps or dark excitons.

Finally, using the DFWM technique, the nonresonant third-order susceptibility $\chi^{(3)}$ of the ZnO nanoparticles (sample 3) was measured to be 6.3×10^{-11} esu. This value, although measured in a very dilute solution, is at least 2 orders of magnitude larger than that of a bulk ZnO sample.

Acknowledgment. This work is supported by RGC grants administered by the UGC of Hong Kong. S.Y. would like to express thanks to the Beijing Synchrotron Radiation Laboratory, Chinese Academy of Sciences, for the supply of beam time.

CM9907817

(36) Adair, R.; Chase, L. L.; Payne, S. A. *Phys. Rev.* B **1989**, *39*, 3342.

(37) Cotter, D.; Ebert, M. G.; Manning, R. J. *Phys. Rev. Lett.* **1992**, *68*, 1200.